CONTROL SYSTEM FOR REAL TIME JITTER REDUCTION AND 3D RECONSTRCUTION OF ROAD PROFILE

by

DIGANT SHAH

Presented to the Faculty of the Graduate School of

The University of Texas at Arlington in Partial Fulfillment

of the Requirements

for the Degree of

MASTER OF SCIENCE IN ELECTRICAL ENGINEERING

THE UNIVERSITY OF TEXAS AT ARLINGTON

AUGUST 2011

ACKNOWLEDGEMENTS

I would like to thank all people who have helped and inspired me during my master's thesis and study work.

I especially want to thank my research advisor, Dr. Roger Walker, for his guidance during my research and study at University of Texas at Arlington. His encouragement, support and enthusiasm made it smooth and easy for me in the preparation and completion of this study. In addition, he was always accessible and willing to help me as well as my colleagues with the research. As a result I was successfully able to complete my research work and write this thesis.

Dr. W. Alan Davis deserves special thanks as my graduate advisor and thesis committee member who always guided me throughout my study here at UT Arlington.

Dr. Jonathan Bredow, the chairman of Electrical Engineering department have been very supportive as my thesis committee member and have offered advice and suggestion whenever I needed them.

All my lab buddies at the Transportation and Instrumentation Laboratory made it a convivial place to work. In particular, I would like to thank Akshay Joshi and Kenan Modi for their help in the past two years. They had inspired me in research and life through our interactions during the long hours in the lab.

Last but not the least; I would like to thank my parents for their support throughout my studies and their faith which made it possible for me to reach at this level.

July 12, 2011

ABSTRACT

CONTROL SYSTEM FOR REAL TIME JITTER REDUCTION

AND 3D RECONSTRCUTION OF ROAD PROFILE

Digant Shah, M.S.

The University of Texas at Arlington, 2011

Supervising Professor: Roger Walker

A large number of bridges, overpasses and other similar structures fail due to deterioration caused by factors such as vehicle loads, impact loads, severe weather conditions, etc. Routine monitoring of such structures is essential to prevent loss of life and property. This thesis explores the feasibility of a 3D bridge monitoring system as a novel way for bridge health analysis. Specifically, the goal of this study is to investigate the use of a video control system for monitoring and synchronize video and surface profile components for a 3D bridge monitoring project.

This thesis focuses on the concept of collecting video data for bridge structure analysis while staying parallel to the road surface and in turn minimizing jitter created by car vibrations. Simulations were performed for examining PID controllers as an option for real time and platform stabilization jitter reduction. The linear relationship which exists between two accelerometers on a rigid bar was verified by conducting an experiment so that need for additional accelerometers for each laser on the 3D profiling system is eliminated. This greatly

reduces the cost of implementing this project. Wide line lasers were simulated and found acceptable components of the monitoring system. A Three dimensional road profile was reconstructed using the raw laser and accelerometer data collected by the Texas Transportation Institute on the test track located at Texas A&M University. Outcomes from experimentation and simulation provided greater insights into using this novel procedure for bridge monitoring.

TABLE OF CONTENTS

LIST OF ILLUSTRATIONS

Figure Page

LIST OF TABLES

CHAPTER 1

INTRODUCTION

1.1 Problem Definition

Most state highway networks include a large number of bridges, overpasses and other similar structures. These structures and roadways deteriorate due to factors such as vehicle loads, impact loads, severe weather conditions, etc.[1]

According to an article on analysis of recent bridge failures in the United States, weather conditions cause almost 53% of all failures. Bridge overload and lateral impact forces from trucks, barges/ships, and trains constitute 20% of the total bridge failures. Other principal causes are design, detailing, construction, material, and maintenance.[2] Since bridge damage and failures due to natural hazards like earthquake and floods are unavoidable, it is still possible to prevent failures due to structural damage. Bridge damage caused by impact loads of trucks, overloaded vehicles, wind, rain and water which causes slow deterioration of the bridge structure can also be prevented with proper maintenance procedures. This kind of slow deterioration can be hazardous if maintenance is not done on a regular basis.

Below are some examples of roadway and bridge failures which happened due to poor maintenance and lack of inspection.

(a)

(b)

Figure 1.1 Bridge and roadway failures due to lack of inspection and bad maintenance. (a) Centennial Bridge Roadway, Panama America (b) Interstate 35W bridge in downtown Minneapolis

Many of these structures are periodically inspected using various methods. To determine whether a structure is still in a serviceable condition, non-destructive test methods (NDT) are used so that maintenance programs can be set up.[3] However, there is always a need for more and better test methods to establish the condition of structures before damage has occurred. Even with the diligent periodic implementation of currently accepted procedures, bridge failures occur.

The 3D bridge monitoring project addresses bridge safety and uses computer-driven technologies to monitor bridge structural and functional changes in order to generate schedules for repairs and maintenance and anticipate risks.

The objective of current research at the Transportation Instrumentation Lab (TIL) at the University of Texas at Arlington (UTA) is to develop a portable embedded, integrated framework that can be used for real-time measuring and monitoring of pavements and bridge deck surfaces at highway speeds as well as monitoring bridge structure changes using image processing techniques. The research conducted in this Thesis is to investigate the feasibility of developing a 3-D pavement profile system for measuring bridge and overpass decks in conjunction with video images of these structures.

1.2 Approach

There are several components involved in implementing the 3D bridge monitoring project. The three main components of the monitoring system are:

- Embedded Transverse Profile System
- Video control system for monitoring and synchronizing video and surface profile
- Structure Image Capture and Processing

The research conducted and described in this thesis focuses on video control system for monitoring and synchronizing video and surface profile component.

One of the ways to reconstruct a road profile in 3D is to use several wide line lasers in a row so that entire lane width is covered and the information of the entire transverse section of

the road is obtained while moving longitudinally. Having the gyroscope on the laser system can give the cross slope and hence we can have all the information to get the 3D profile of the road.

To get the best estimate of the bridge structures all the data should be in reference to the road surface. By knowing the 3D of the road profile we can make the camera platform line up with the road surface in real time. 3D surface profile can be measured using the laser profiling system which consists of line lasers, accelerometers and gyroscopes, and road profile measurement. Adding the video data of the bridge structures while following the road profile can be done by having a control system that would control the camera platform position and line it up with road surface.

Further chapters of the thesis include an introduction to control systems and its use for platform stabilization as mentioned in the above paragraph, and simulation and results supporting the implementation of some essential parts of the 3D bridge monitoring system.

CHAPTER 2

3D PROFILING

2.1 Introduction to 3D profiling and past work

2.1.1 Road profiling

Road profile is the 2D cross section of a road surface taken along an imaginary line. Profile gives information about roughness, design grade and texture of the road.[4] When testing a road for roughness, most of the profiling companies and state transportation departments measure the longitudinal profile of the road.

The International Roughness Index (IRI) is computed from the road profile. It is used as an indicator of the roughness of the road surface. It is commonly expressed in units of mm/m, in/mi, etc.[5] Maintenance and repairs of the road can be carried out if the IRI of the road is more than the standard or as decided by the state transportation department.

Many state transportation agencies and profiling companies use lasers and accelerometers for measuring the profile. A profiling algorithm is used to filter out the car movement from the laser/accelerometer readings. The next section describes an algorithm developed and used at TIL for computing the profile from these sensors.

2.1.1.1 Profiling Algorithm

An explanation of how profile is computed using the profiling algorithm is given in this section.

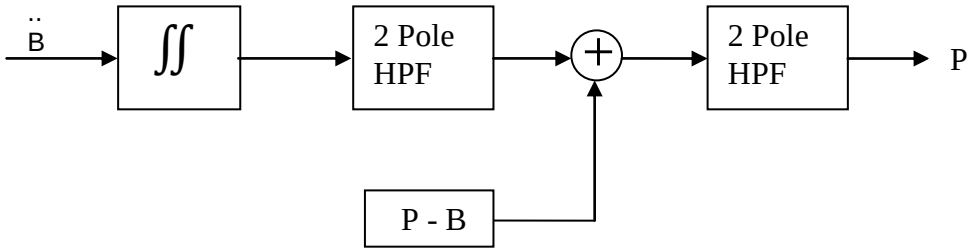

Figure 2.1 Block diagram of profiling algorithm

..
B = Accelerometer

P - B = laser

$$\iint \ddot{B} + [P - B] = P \qquad (2.1)$$

Taking the double integration of the accelerometer and filtering out the long wavelengths using the two pole high pass filter gives the movement of the car in terms of displacement. Taking this displacement and adding it to the laser will give the elevation of the road surface. To filter out the offset from the profile and to get an accurate measurement, another two pole high pass filter is used during the last stage.

When combining the accelerometer W(z) with laser X(z) the following result are obtained.

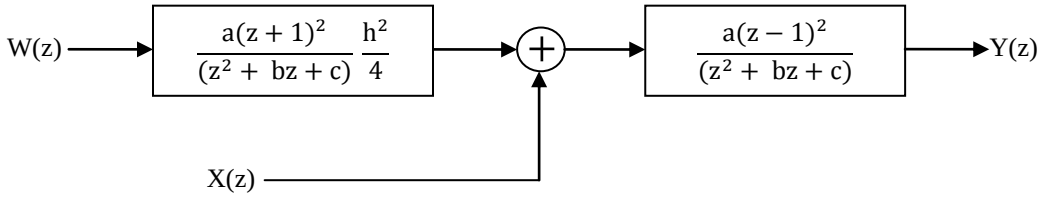

Figure 2.2 Transfer function diagram of profiling algorithm

$$Y(z) = W(z) \frac{a(z+1)^2}{(z^2+bz+c)} \frac{h^2}{4} + X(z) \frac{a(z-1)^2}{(z^2+bz+c)} \qquad (2.2)$$

Time is used as a base for the calculation of the profile with the finished algorithm, as shown below.

$$Y_t = - bY_{t-1} - c\,Y_{t-2} + \frac{ah^2}{4}(W_{t-2} + 2W_{t-1} + W_t) + a(X_{t-2} - 2X_{t-1} + X_t) \quad (2.3)$$

2.1.2 3D Profiling

The transverse profile of the road is determined using a parallel set of longitudinal profiles along with the slope of the road. The 3D profile can serve as a means of analyzing the road surface more accurately, so that areas where grind and fill is necessary can be known and other details can be found out which are not possible by simply looking at the longitudinal road profile.

To get an accurate 3D profile of the road, the car movement should be taken out from the laser readings. This task is successfully done for longitudinal profile measurements. The same procedure is applied to a transverse profile. The transverse profile is then adjusted with the cross slope measurement from the gyroscope.

2.1.2.1 Past development in 3D profiling [6]

Previous research has been done at Transportation and Instrumentation Laboratory in developing a system which can give three dimensional road profile. The system included an inertial profiler, a scanning laser or the use of multiple single point lasers and a two or three axis gyroscope for computing the 3D profile of the road. This system was developed for measuring rut or determining the grind and fill areas on the road so that repairs can be done for maintenance and thus acceptable International Roughness Index (IRI) is obtained.

Some implementation details for the scanning laser is described in this section.

A static scanning laser was used so that it scans the transverse section of the road covering the entire lane width. The figure below shows a slice of the scanning laser where P_{left} is the left profile, P_{right} is the right profile and the θ is the cross slope.

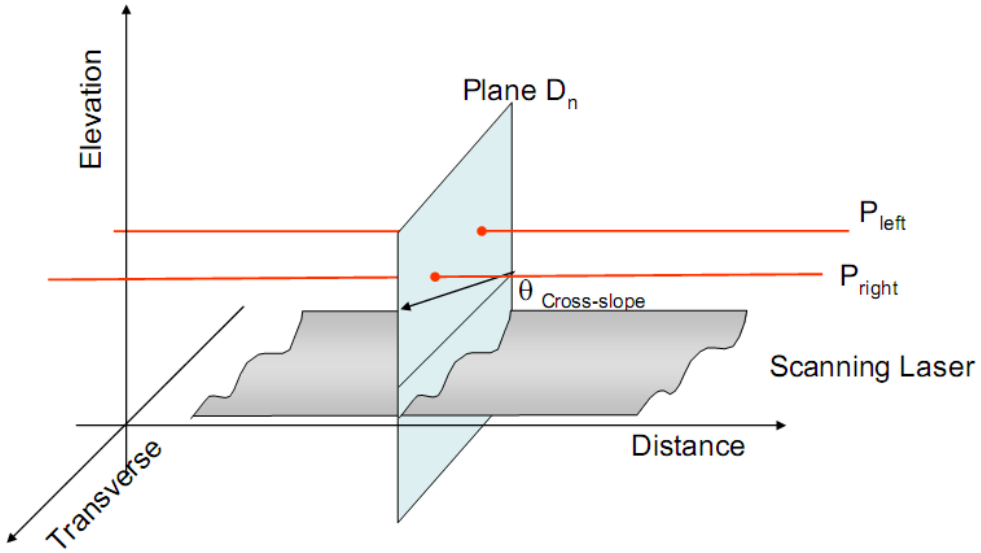

Figure 2.3 Slice of Scanning Laser

To get the estimate of the road profile for that section we gather all the data along the road surface. The surface data taken by the scanning laser and the profile measured by the inertial profiler are rotated at the angle given by the gyroscope sensor and the offset, which is the distance between the laser and the road surface.

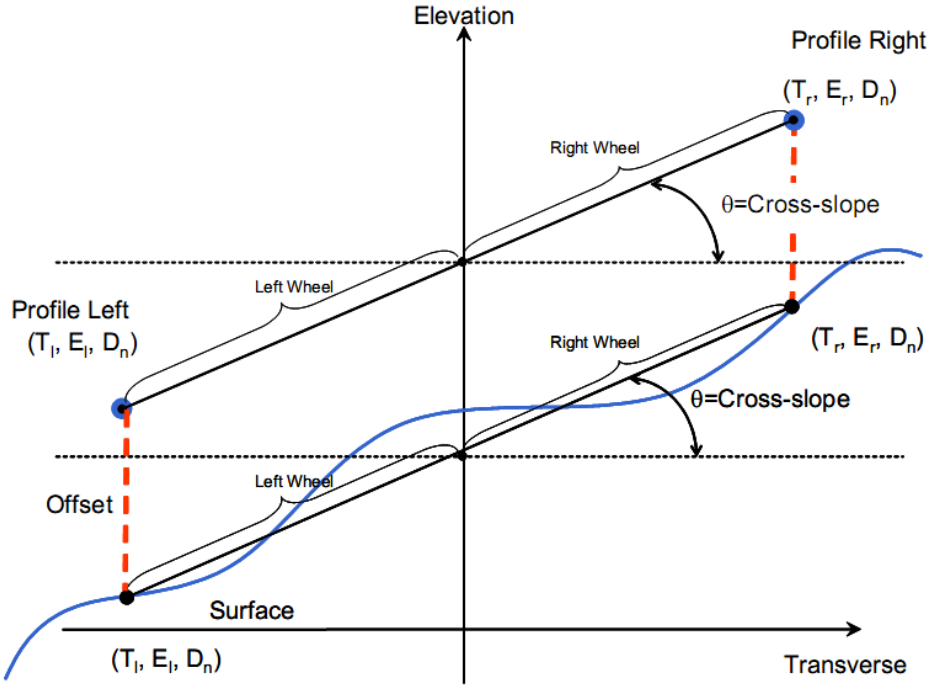

Figure 2.4 Rotating and Offsetting the Scanning Laser to Match Rotated Profile

The scanning laser was tested on a specially built pavement with different rut depths. Rutting was introduced in three different bump depths along each wheel path. One of the wheel path areas with rutting going from 0 to 0.5 and 0.5 to 1 inches is shown in the figure below. The rut depth is changed at 10 feet which is marked by the white line in the figure. The 3D profile of the same is shown in the figure 2.5, where the black transverse sections mark the partition of the two rut depths, i.e., from 0 to 0.5 and the 0.5 to 1 inch rut depth sections.

(a)

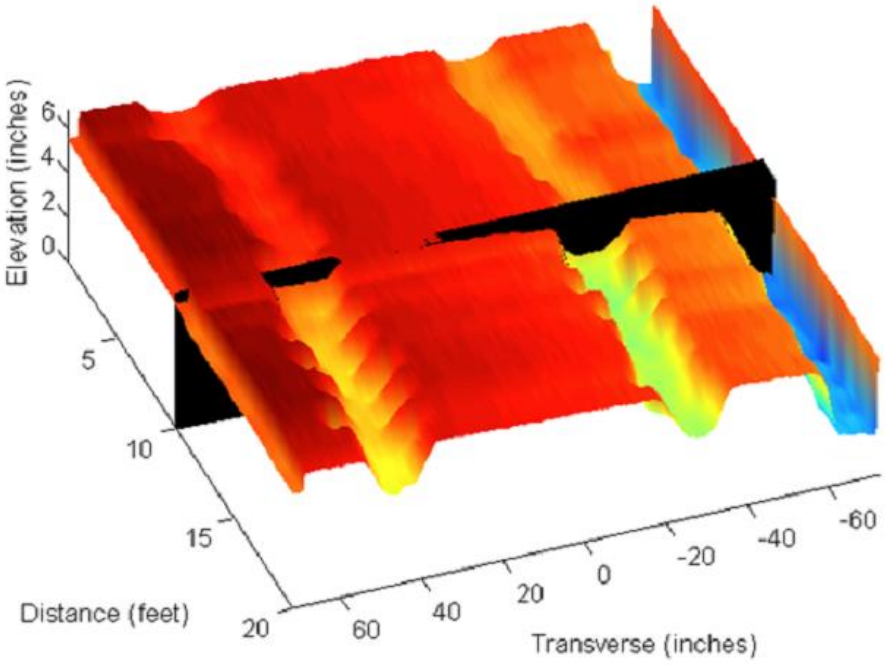

(b)

Figure 2.5 (a) 0 to 0.5 and the 0.5 to 1 inch rut depth sections (b) 3D profile for the 0 to 0.5 and the 0.5 to 1 inch rut depth sections

2.1.2.2 Introduction to 3D bridge monitoring system

As static instruments cannot be used for road profile measurement of highways and areas with high speed traffic, a system needs to be developed which can measure the road profile at highway speeds. The 3D bridge monitoring project using the wide foot print lasers will not only be useful for low speed measurements but can also be used at high speeds and thus have the capability of monitoring the condition of bridge structures.

The 3D bridge monitoring system uses like wide line lasers, accelerometers, gyroscopes and a camera on a platform mounted on the car along with the platform stabilization system. The video data from the camera is used for identifying the structures of the bridge. The video images are then integrated with the 3D road bridge deck surface to form a complete 3D structure of the bridge. The 3D data can be taken periodically and compared with previous readings to find any unusual structural changes so that necessary steps can be taken if the changes are not acceptable.

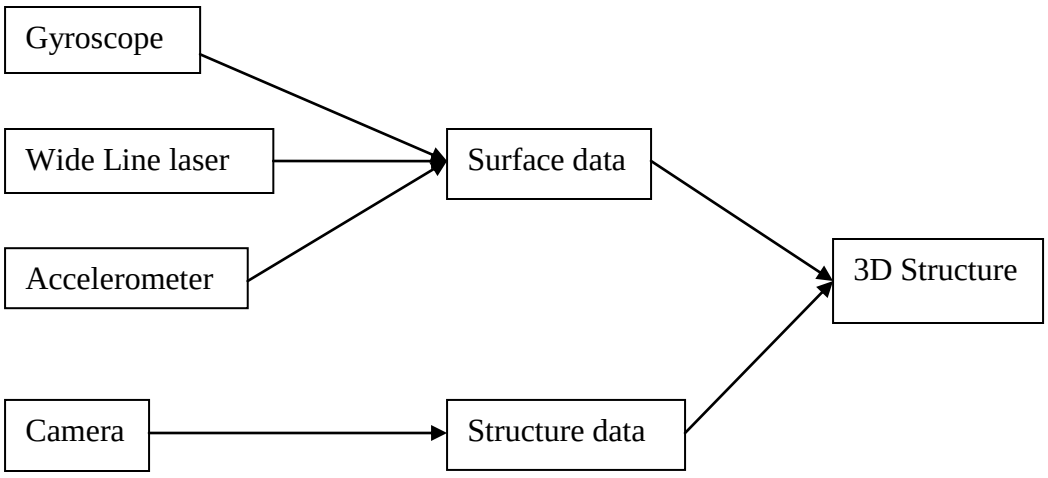

Figure 2.6 Integration of sensors for 3D reconstruction

Figure 2.7 shows how the gyroscope, the line lasers and the camera are configured on the vehicle used to collect the 3D data.

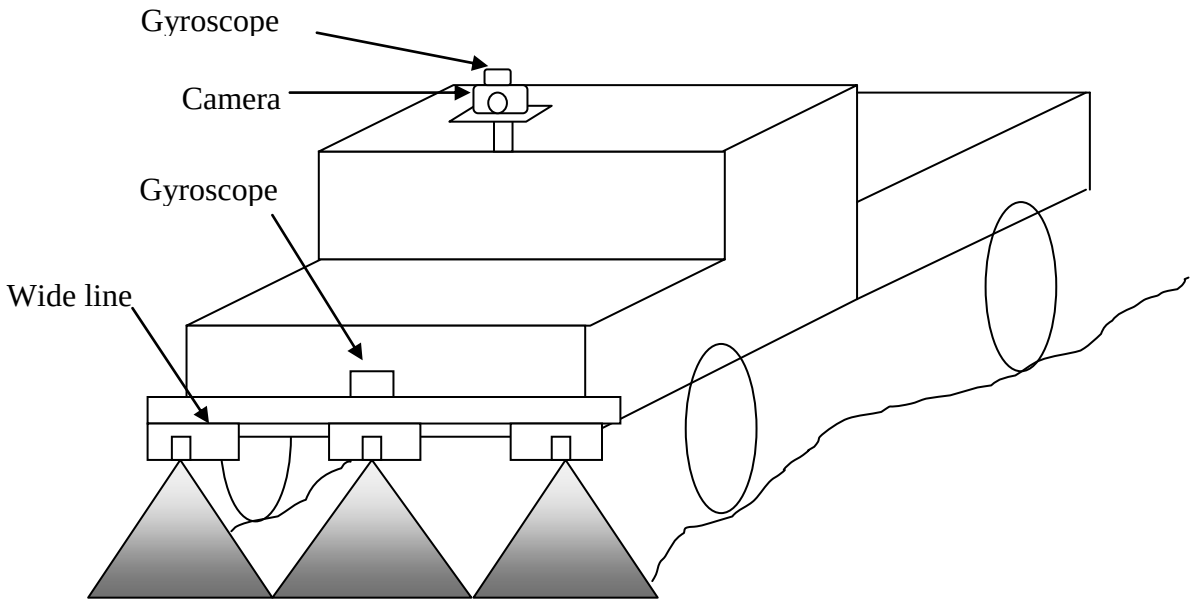

Figure 2.7 Setup for 3D bridge monitoring system

Recently developed Wide Line lasers are useful in road profiling as they can provide multiple transverse scans as the vehicle travels down the road thus providing a set of longitudinal readings. Newly developed lasers are expected to be able to scan around 1 meter of readings. Thus by installing 4 or 5 wide line lasers in a row the entire lane width of the road can be measured. The lasers are typically installed on a frame or a bar on the front side or rear side of the vehicle.

A 2- axis or 3-axis gyroscopes can be used to get the angular rotation for determining the slope of the road along the x, y and z axis needed for the 3D reconstruction of the road profile. A second gyroscope on the camera platform is used to make the platform stay in line with the road profile and counter the jitter produced by the body of the car.

A video camera is used to get the video data of the bridge structures so as to compare for determining the structures of the bridge or overpass. This data can then be compared with previous readings,.

The CCD camera which is synchronized with the wide line laser can take the video of the bridge structure. The following three steps are proposed for getting a proper measurement to finalize the predictions:

1) Image matching and registration :

Because the bridge's images are captured at different times, locations, and angles, they must be registered before comparison is made to measure the structures' parameters. Moreover, for some large bridges, one image cannot show the complete structure and several images from different views should be integrated to get the bridge image. It is necessary to use image matching techniques to combine information of several small images.

2) Bridge structure detection :

Previously registered images can be used to compare with the new results and find out the changes in the structure. Most of the bridge structures e.g. beams are straight lines and with the help of image processing techniques, all the edges and straight lines in the image can be determined. Then matching can be done with the corners and the lines of the previously registered image. This is used to determine if there are any changes along with how much the structure has changed from its previous position.

The figure 2.8 shows how the edges and the lines of the bridge structures are detected by using the image processing techniques like canny edge detection and Hough transform.

(a)

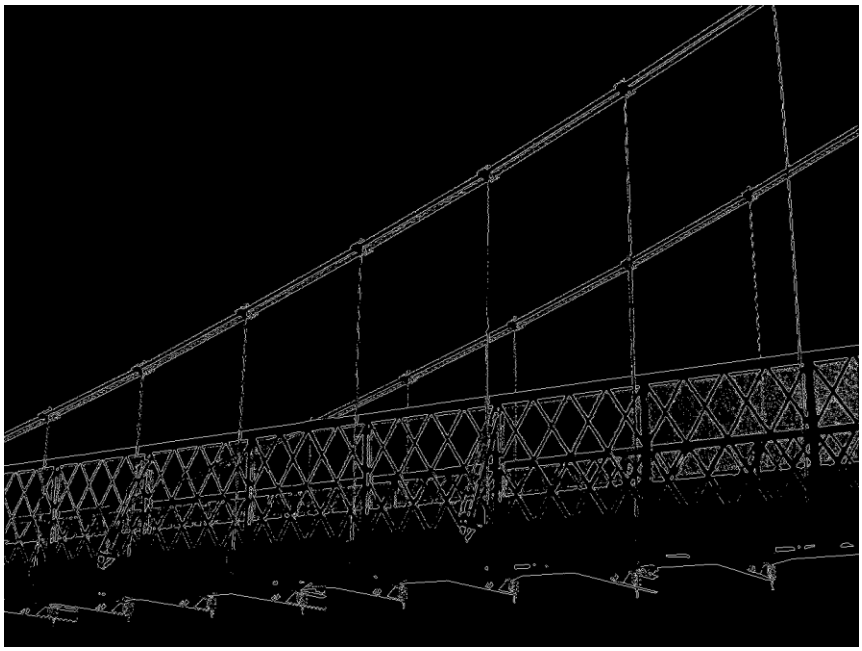

(b)

Figure 2.8 (a) Image of a bridge (b) Edges of the structures extracted by using image processing techniques

3) Measurements :

After registering images and detecting structures, the changes of structures between images can be measured. Measuring needs to be done for the checking distances between the boundaries of structures to see if there are slides within bridge structures. Because the camera is synchronized with the 3D laser system, comparison of the image based measurements to 3D surface changes can be carried out for the final decision.

As noted from the above description accurate road or surface profiling methods exists. Technology in the use of CCD video imaging for bridge structures is in the early stages of development. Combining and synchronizing bridge deck profile surface data with CCD video imaging for bridge structural characteristics has not been performed.

CHAPTER 3

CONTROL SYSTEM FOR REAL TIME MOTOR POSITION CONTROL

This chapter includes an introduction to control system concepts, Proportional-Integral-Derivative (PID) controller, controller simulation, and results of motor position control. The PID controller is used in the bridge monitoring system for proper positioning of the camera and minimizing camera jitter.

3.1 Introduction to Control system and PID controller

3.1.1. Control System

A device or set of devices used to manage, command, direct or regulate the behavior of other devices or systems is called a control system. Logic or sequential control systems, linear or feedback control systems and fuzzy logic control systems are some of the examples of different control systems.[7] The term "control system" may be applied to the essentially manual controls that allow an operator, for example, to close and open a hydraulic press, perhaps including logic so that it cannot be moved unless safety guards are in place. An automatic sequential control system may trigger a series of mechanical actuators in the correct sequence to perform a task. For example various electric and pneumatic transducers may fold and glue a cardboard box, fill it with product and then seal it in an automatic packaging machine. In the case of linear feedback systems, a control loop, including sensors, control algorithms and actuators, is arranged in such a fashion as to try to regulate a variable at a setpoint or reference value.

The controller in open loop control system determines the input signal to the process by reference signal only and the controller in a closed loop system determines the input signal to

the process on the basis of measurement of the output of the process (i.e. feedback signal) along with the reference signal.[8]

A feedback control method has had a tremendous impact in many disciplines such as engineering, biological sciences, business, and economy. Feedback control monitors the output and according to that it generates new input signals such that the effect of disturbances is compensated and desired response is obtained.[9] The availability of control system components at a low cost has favored the increase of the applications of the feedback principle (for example in consumer electronics products).

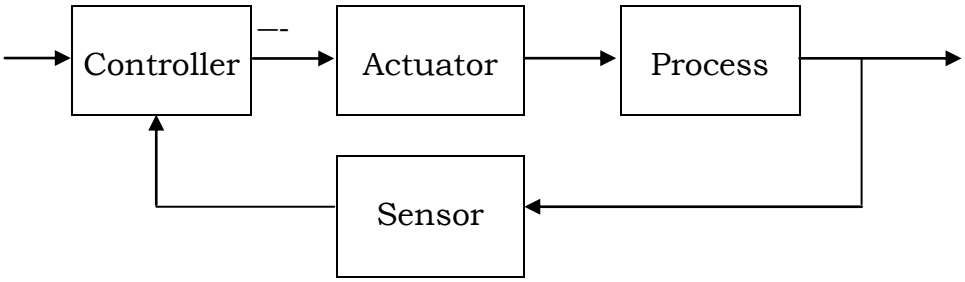

Figure 3.1 Feedback control loop[9]

3.1.2. PID Controller

In almost all process industries the PID algorithm is used for control, and it serves as a basis for many other advanced control algorithms and strategies. The PID controller has been in use for over a century in various forms. It has enjoyed popularity as a purely mechanical device, as a pneumatic device, and as an electronic device. While the actual digital implementation of the PID algorithms has changed and it is different for different systems and commercial equipment, there is no change in the basic algorithm for years and it is used in all distributed control systems.[10]

The digital PID controller using a microprocessor has recently come into its own in industry. It is also straight forward task to embed a PID controller into a code. PID stands for

"proportional, integral, derivative." These three terms describe the basic elements of a PID controller. Each of these elements performs a different task and has a different effect on the functioning of a system. In a typical PID controller these elements are driven by a combination of the system command and the feedback signal from the object that is being controlled. Their outputs are added together to form the system output.[11]

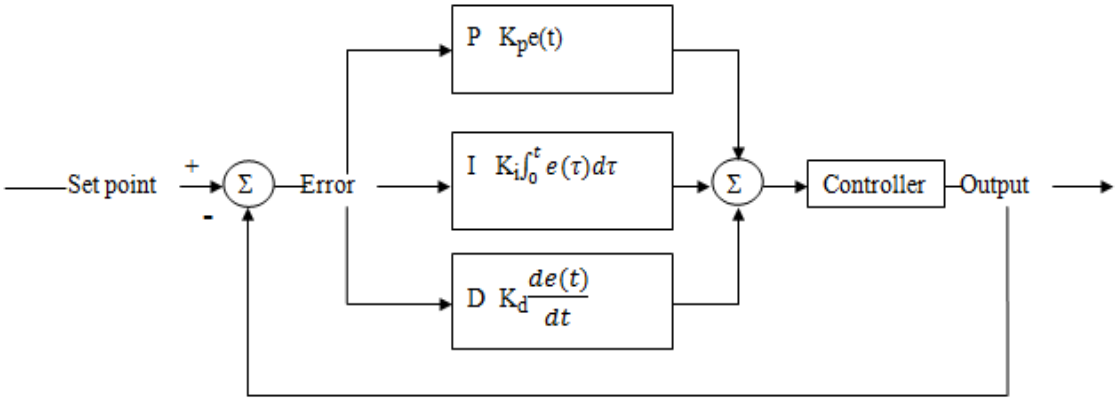

Figure 3.2 PID control loop

The manipulated variable, which is the input to the process, is calculated as the sum of proportional, integral and derivative terms.

$$MV(t) = K_p e(t) + K_i \int_0^t e(\tau)d\tau + K_d \frac{de(t)}{dt} \quad (3.1)$$

A proportional controller is just the error signal multiplied by a constant and fed out to the drive. Larger values of proportional gain typically mean faster response since the larger the error, the larger the proportional term compensation. An excessively large proportional gain will lead to process instability and oscillation.

Integral control is used to add long term precision to a control loop. It is almost always used in conjunction with proportional control. It deals with the past values of the errors. Larger values of integral gain imply steady state errors are eliminated more quickly. The trade-off is a

larger overshoot, where any negative error integrated during a transient response must be integrated away by a positive error before reaching steady state.

Derivative control is a predictive control which predicts the behavior of the plant and is used to stabilize the plant. Larger values of the derivative gain decreases overshoot, but slow down transient response and may lead to instability due to signal noise amplification in the differentiation of the error.

As seen above the PID controller is a very simple yet effective control method that can be used for the purpose of jitter reduction and platform orientation control in real time. This is one of the possible implementations for the control system in the video collection unit of the 3D bridge monitoring system.

3.2 Control system for real time platform stabilization

As discussed previously, there is a need for getting the video information of the bridge structures with minimum jitter while following the road profile which is not perfectly horizontal. A control system which controls the position of the platform on which the camera is mounted is required for getting the accurate video data. The control system would be positioning the platform in such a way that the disturbance or the vibration created by the car movement is compensated as well as the platform stays in line with the road profile. A PID controller can be used for carrying out the above mentioned task.

Platform needs to be stabilized in real time so as to get accurate video information from the camera. Assuming that the camera used on the platform would be running at the maximum 30 fps capture rate, which is more than enough to fulfill the requirements of the image processing part of the project, the platform must be stabilized in less than 33.33 msec each time. So the first criterion to be taken into consideration is the settling time of the system. Also, the overshoot for the system response should be decided and should not be more than 10% of the total change in the set point value.

The control system would get the data from two gyroscopes one of which is on the frame where the profiling sensors are mounted and the other on the platform in line with the camera axis.

Suppose the gyroscope on the camera platform will be giving the angle θ1 because of the vibrations of the body of the car and the gyroscope on the front bar will be giving the slope of the road. Following the road surface, the angle θ2 should be the platform angle and θ1 needs to subtracted as it the jitter due to car vibrations. So the actual angle that the platform should be rotated with respect to horizontal is:

$$\theta = \theta 2 - \theta 1 \qquad (3.2)$$

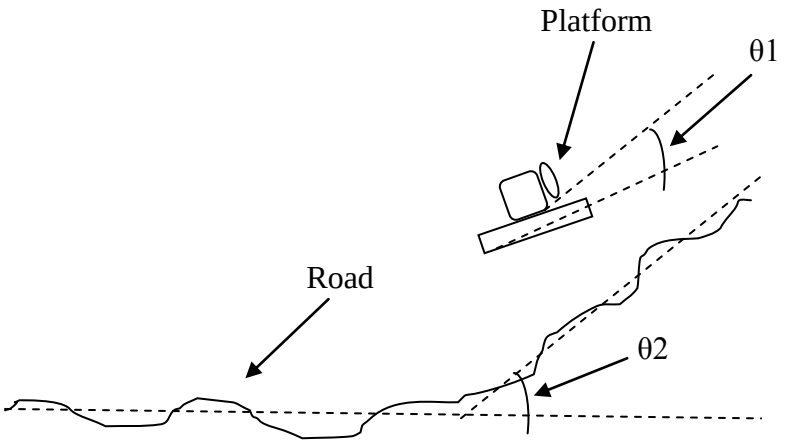

Figure 3.3 Angles measured by the two gyroscopes

This angle will be the input to the controller and corresponding controller output will make the motor move eventually bringing the platform in line with the road slope and compensating for the car vibration.

3.2.1. Simulation of Motor position control in Simulink

Simulation for the motor position control was carried out to verify the effectiveness and performance of the PID controller as an option for controlling the camera platform.

Motor modeling and PID controller analysis was done in Simulink. The stepwise procedure for motor modeling and implementing the PID controller is described below.

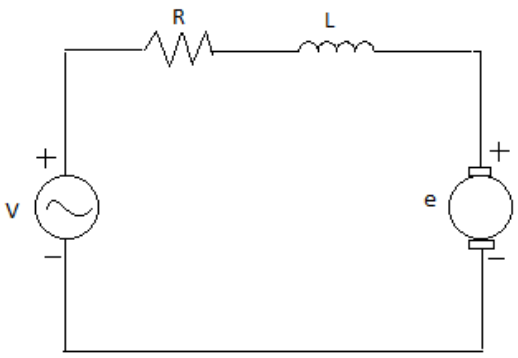

(a)

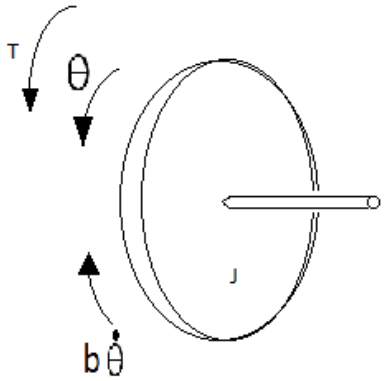

(b)

Figure 3.4 (a) Electric circuit of the armature of a dc motor (b) Free body diagram of the rotor

In the above figures the electric circuit of the armature of a dc motor is shown where there is the electrical resistance, motor induction and back emf of the motor is shown. The rotor diagram shows the direction of torque in the direction of the rotation and the opposing force b*(dθ/dt)

The modeling of a motor can be done by using Newton's equation in combination with Kirchhoff's law.

$$\frac{d^2\theta}{dt^2} = \frac{1}{J}\left(K_t i - b\frac{d\theta}{dt}\right)$$ [12] (3.3)

Where,

J – Moment of inertia

$\frac{d^2\theta}{dt^2}$ – Angular acceleration

T – Torque

b – Damping coefficient of the mechanical system

$\frac{d\theta}{dt}$ – Angular acceleration

K_t – Motor coefficient

i – Armature current

Value of θ is obtained by double integrating the equation (3.3).

Also,

$$\frac{di}{dt} = \frac{1}{L}\left(-Ri + V - K_e\frac{d\theta}{dt}\right)$$ [12] (3.4)

Where,

L – Motor electrical inductance

R – Electrical Resistance

V – Supply voltage

K_e – Motor constant

The current is obtained by integrating the equation (3.4).

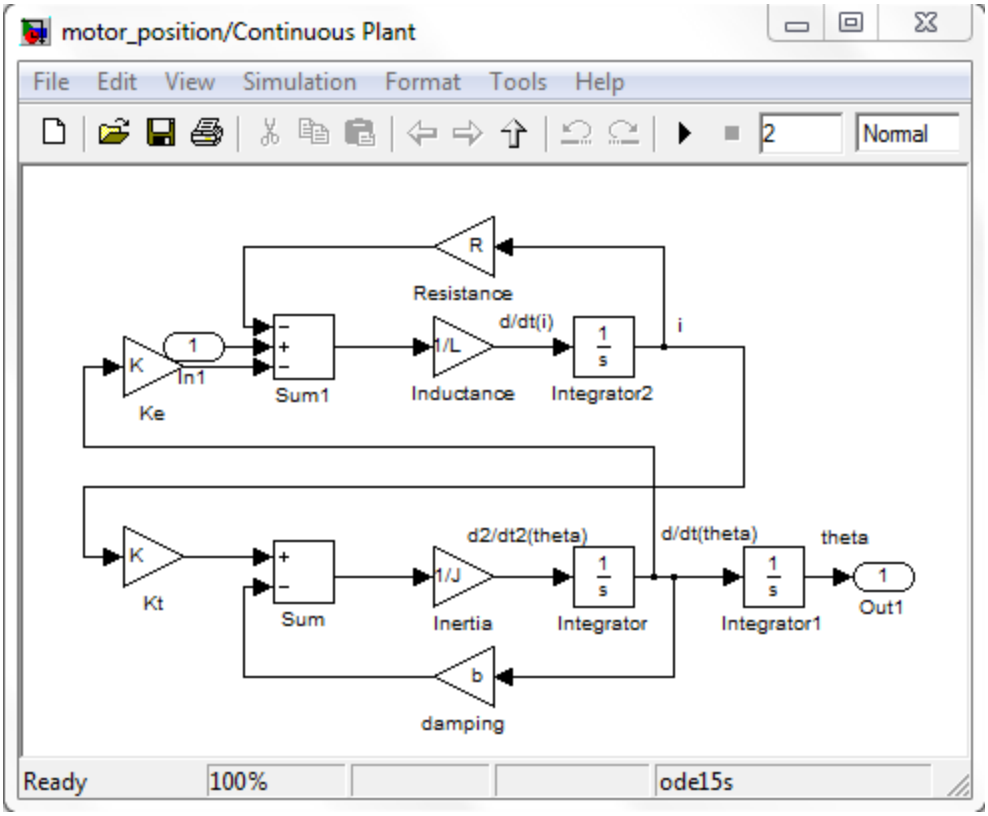

Figure 3.5 Motor model in Simulink

The motor parameters used for simulation purposes were actual parameters obtained by experimentation done in Carnegie Mellon's undergraduate controls lab.

J (moment of inertia of the rotor) = 3.2284E-6 kg.m^2/s^2

b (damping ratio of the mechanical system) = 3.5077E-6 Nms

K=Ke=Kt (motor constant) = 0.0274 Nm/Amp

R (electric resistance) = 4 ohm

L (inductance) = 2.75E-6 H

By using the digital linear model function (dlinmod) and state space to transfer function (ss2tf) in Matlab, the discrete transfer function of motor model is obtained.

```
>> [A,B,C,D]=dlinmod('motor_model', .001)
A =   1.0000    0.0000    0.0010
        0   -0.0000   -0.0065
        0    0.0055    0.9425
B =   0.0010
      0.2359
      2.0589
C =   1.0000         0         0
D = 0

>> [num,den]=ss2tf(A,B,C,D)
num =   0    0.0010    0.0010    0.0000
den =    1.0000   -1.9425    0.9425         0
```

Thus the discrete transfer function of the motor model obtained is

$$\frac{0.001z+0.001}{z^2-1.9425z-0.9425}$$

Since the motor is modeled, a controller is required so that the position of the shaft of the motor can be controlled. For the simulation purpose digital PID controllers were used to check and compare the performance of the system.

Digital PID controller in ‘z’ domain can be written as

Proportional (P): $C(z) = K_p E(z)$ (3.5)

Integral (I): $C(z) = \frac{K_i Ts\, z}{z-1}$ (3.6)

Derivative (D): $C(z) = \frac{K_d (z-1)}{Ts\, z}$ (3.7)

Thus,

PID = $K_p E(z) + \frac{K_i Ts\, z}{z-1} + \frac{K_d (z-1)}{Ts\, z}$ (3.8)

The discrete PID controller given in equation 3.8 can be built by using the blocks from the simulink library browser. Gain blocks are used for Kp, Ki and Kd gains while discrete transfer function blocks are used to have integral and derivative controller in Z transform. The sampling time, Ts, and the parameters Kp , Ki and Kd are required to be tuned so as to get the desired response.

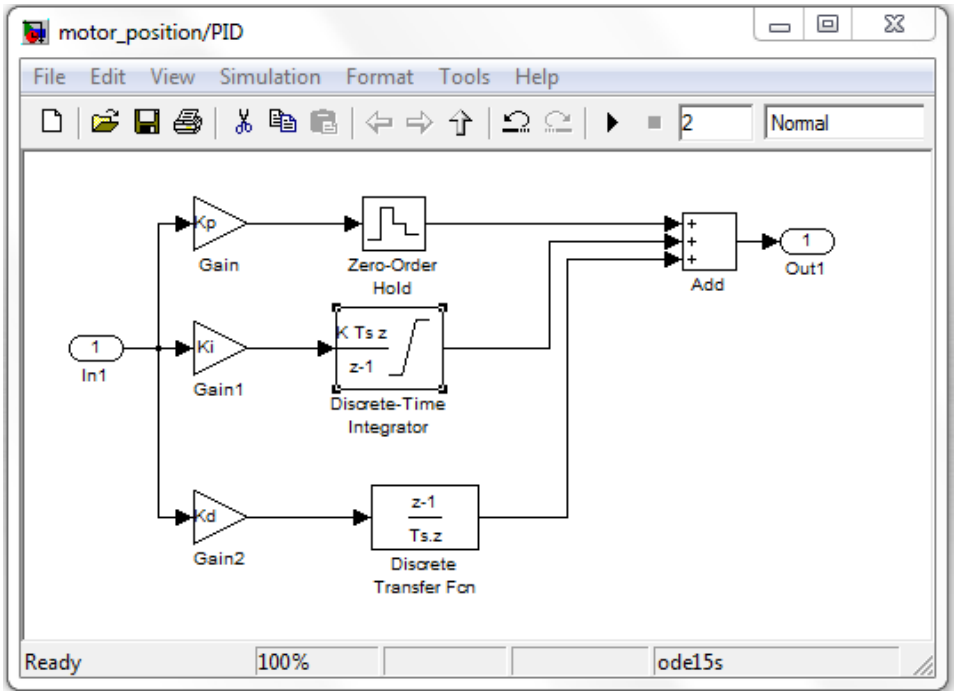

Figure 3.6 Discrete PID controller

The inbuilt discrete PID controller block can be found from the Discrete Control block section of the Extra library sub part of the SimPower Systems blocks. It has different transfer functions used for the integral and derivative term than that of the PID controller described above.

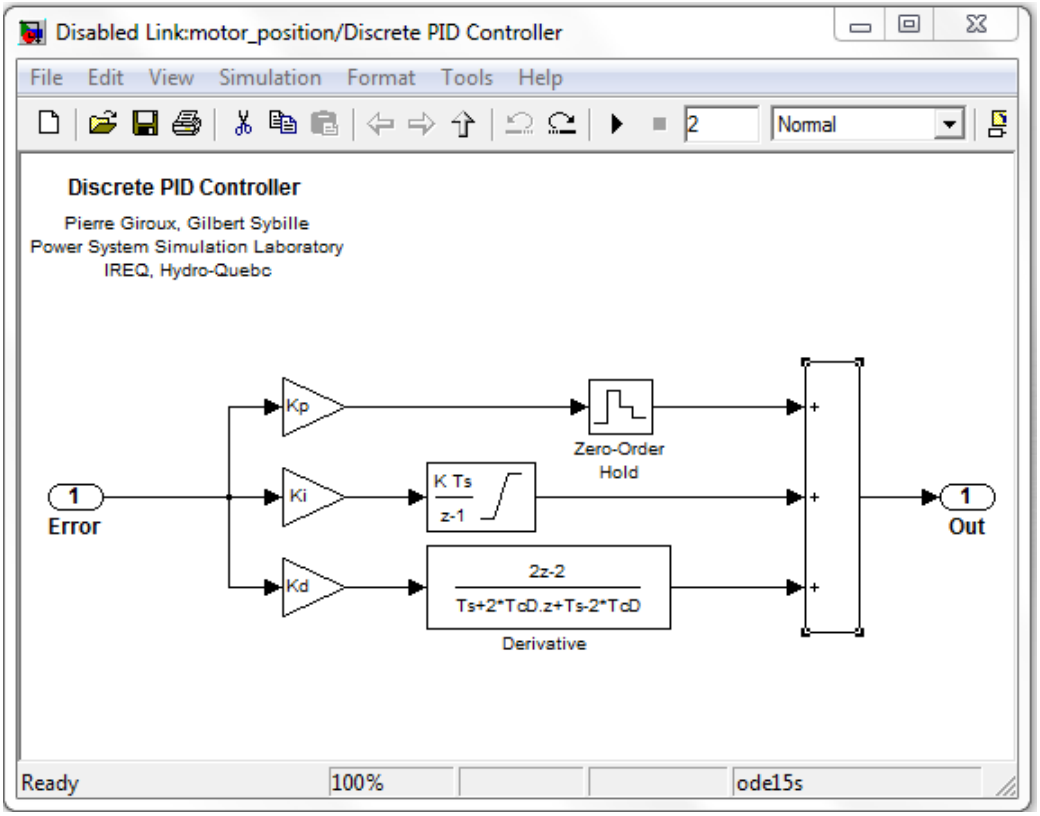

Figure 3.7 Inbuilt discrete PID controller from simulink library

For tuning the PID controller there are different methods and algorithms which can be used. There are different algorithms like Ziegler–Nichols, Cohen-Coon, etc. that can be used for the purpose of tuning the PID controller. The Ziegler–Nichols method was used to get a rough estimate and then the trial and error method was used to get proper value of gains for this simulation. Different motors will have different electrical and physical characteristics and so the gains derived in this simulation will not remain the same for all cases.

There were three different inputs given to the PID controller which acts as the setpoint changes.

(1) Unit step input – A normal unit step function which acts as 1 radian setpoint change.

(2) A predefined time and amplitude input – This input generates the step change at predefined time with predefined amplitude by looking at the lookup table defined by the user.

(3) Varying frequency with fixed amplitude input – The input pulse frequency changes from 7.5 Hz to 15 Hz in 2 seconds time and it has fixed amplitude of 2 radians.

A unit step response of the system can be taken so that the gains can be set and the PID controller can be tuned to get the desired response. For both of the PID controllers mentioned above, gains were set to appropriate values considering the settling time and the maximum overshoot requirements of the response. Gain values obtained are given in the table below.

Table 3.1 Gain values for PID controllers

	Discrete PID	Inbuilt PID block
Kp	15.32	4.7
Ki	5.3278	0.035
Kd	0.25	0.06875

The figure 3.8, 3.9 and 3.10 show how the motor model is setup for simulation and plots show the unit step response of the system using both PID controllers.

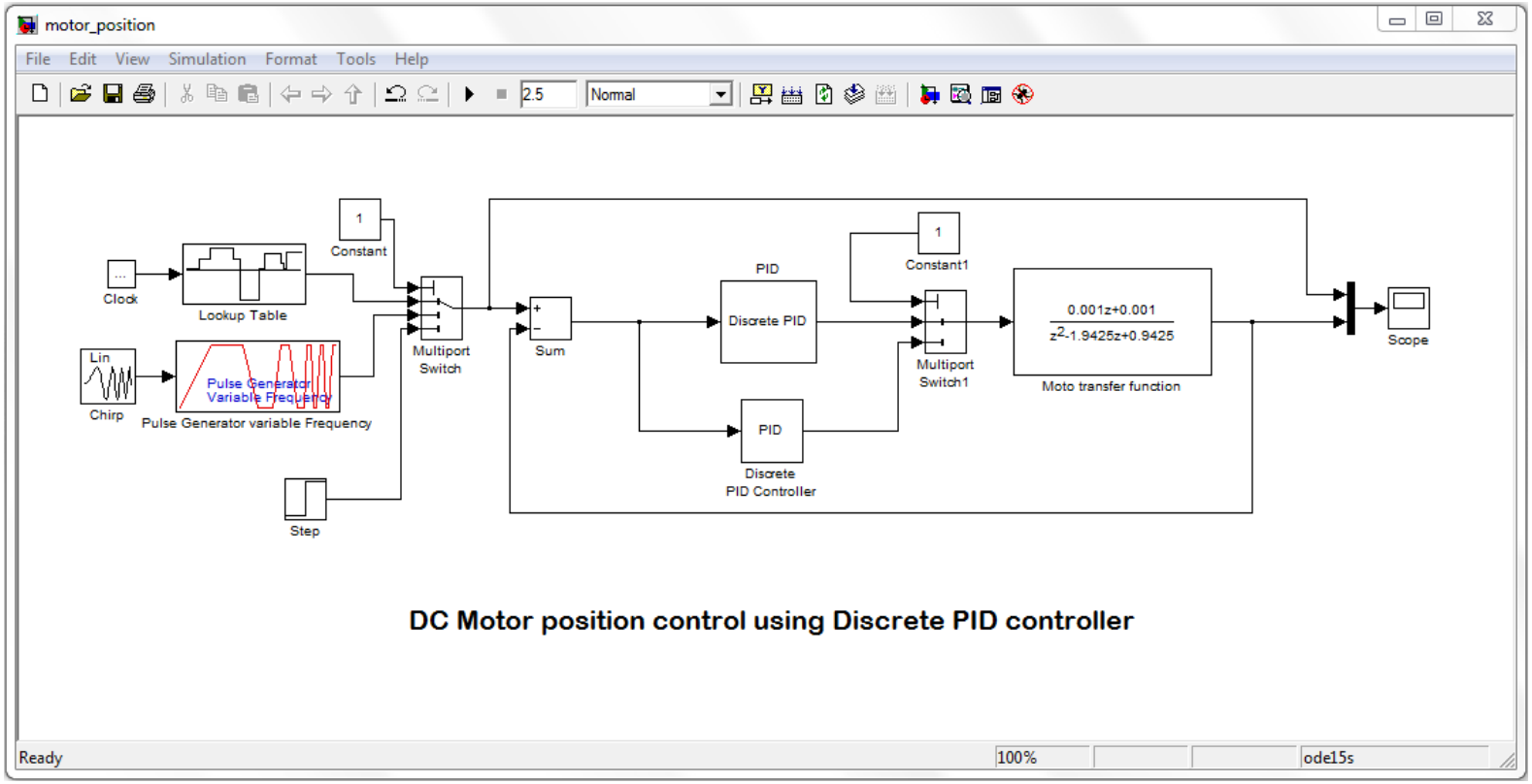

Figure 3.8 Simulink setup for simulation of motor position control

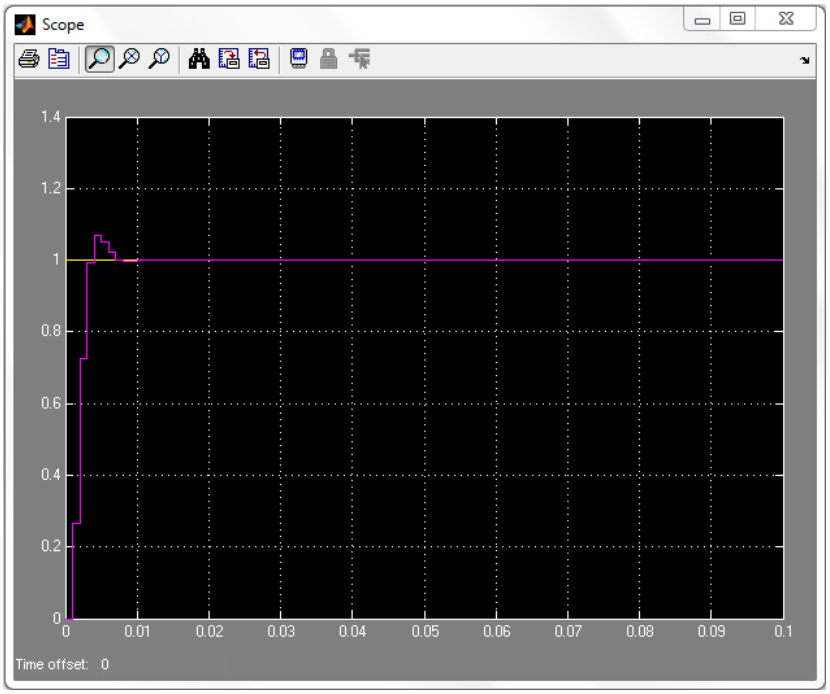

(a)

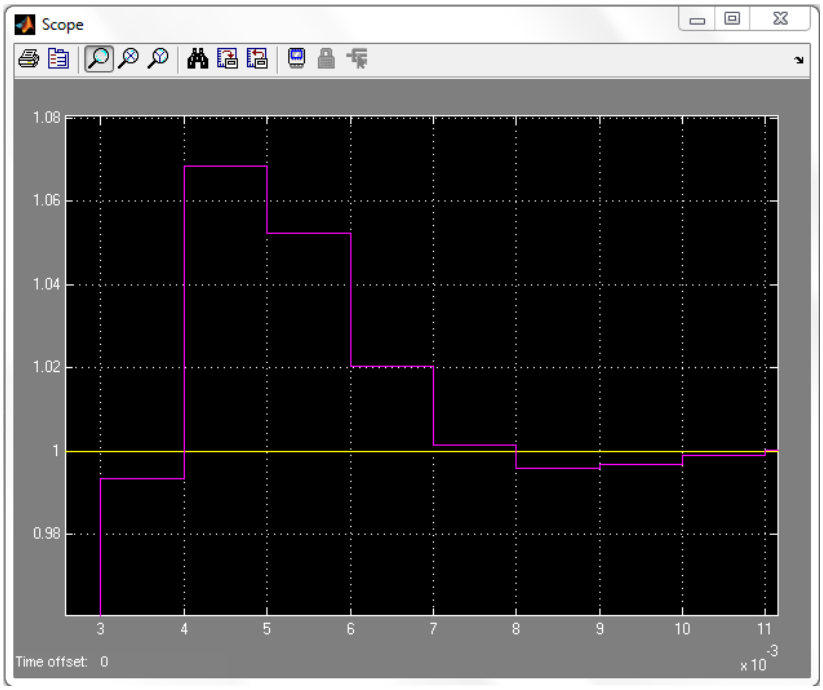

(b)

Figure 3.9 (a) Unit step response of the system (b) Zoomed view of unit step response

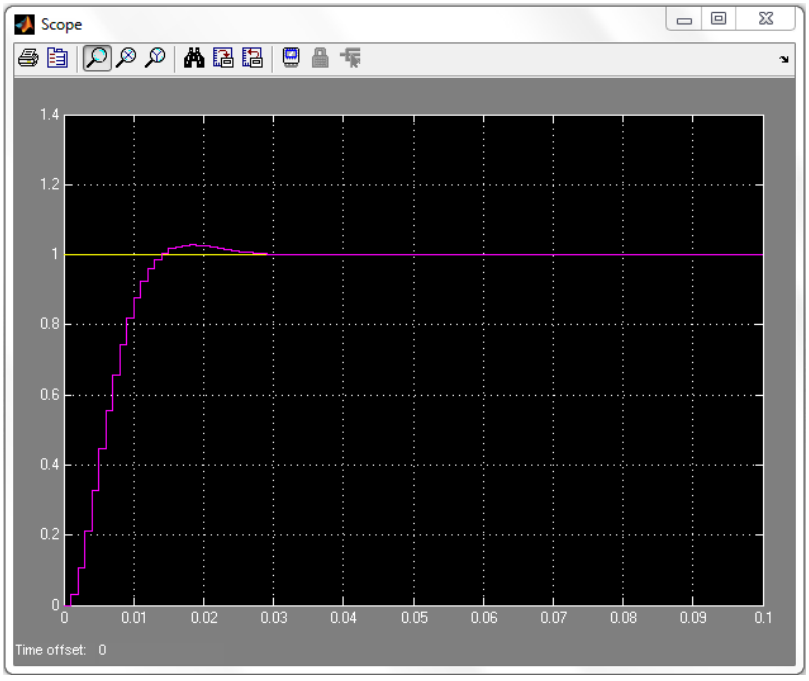

(a)

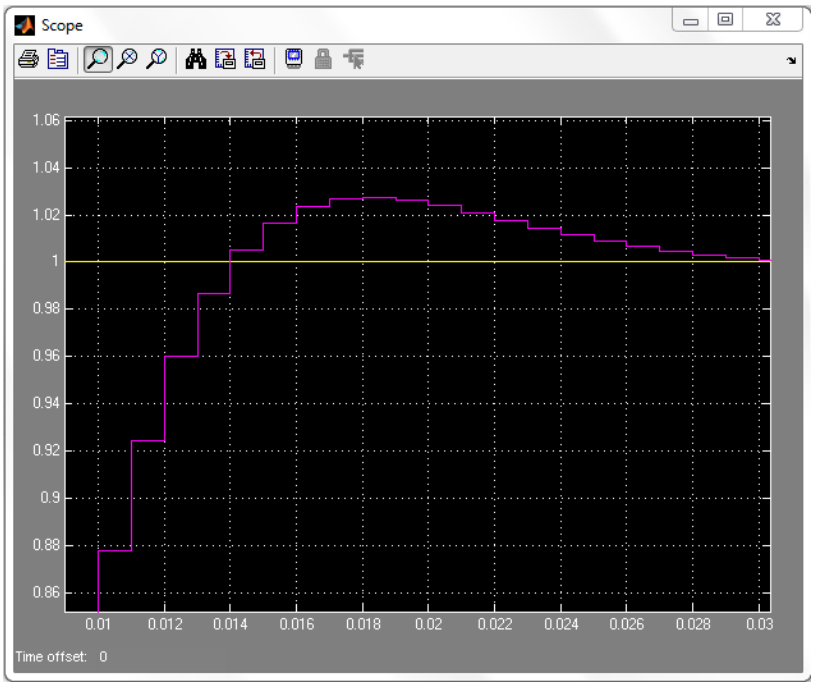

(b)

Figure 3.10 (a) Unit step response of inbuilt PID block (b) Zoomed view of unit step response

As seen in the above figures the settling time of the response for the discrete PID controller is 11 x 10^{-3} seconds which is almost one third of maximum settling time defined and the overshoot is approximately 7% of the total set point change which is less than the maximum overshoot criteria of the system response.

For the inbuilt PID block the settling time as seen from the simulation results came out to be 30 x 10^{-3} seconds which is also less than the maximum settling time and overshoot of the response is approximately 3% of the total set point change.

In the following figures it can be seen that both of the controllers follow the input very well and even at 15 Hz frequency with two radians of set point change, the response of the system satisfies all the conditions that will allow the system to work in real time.

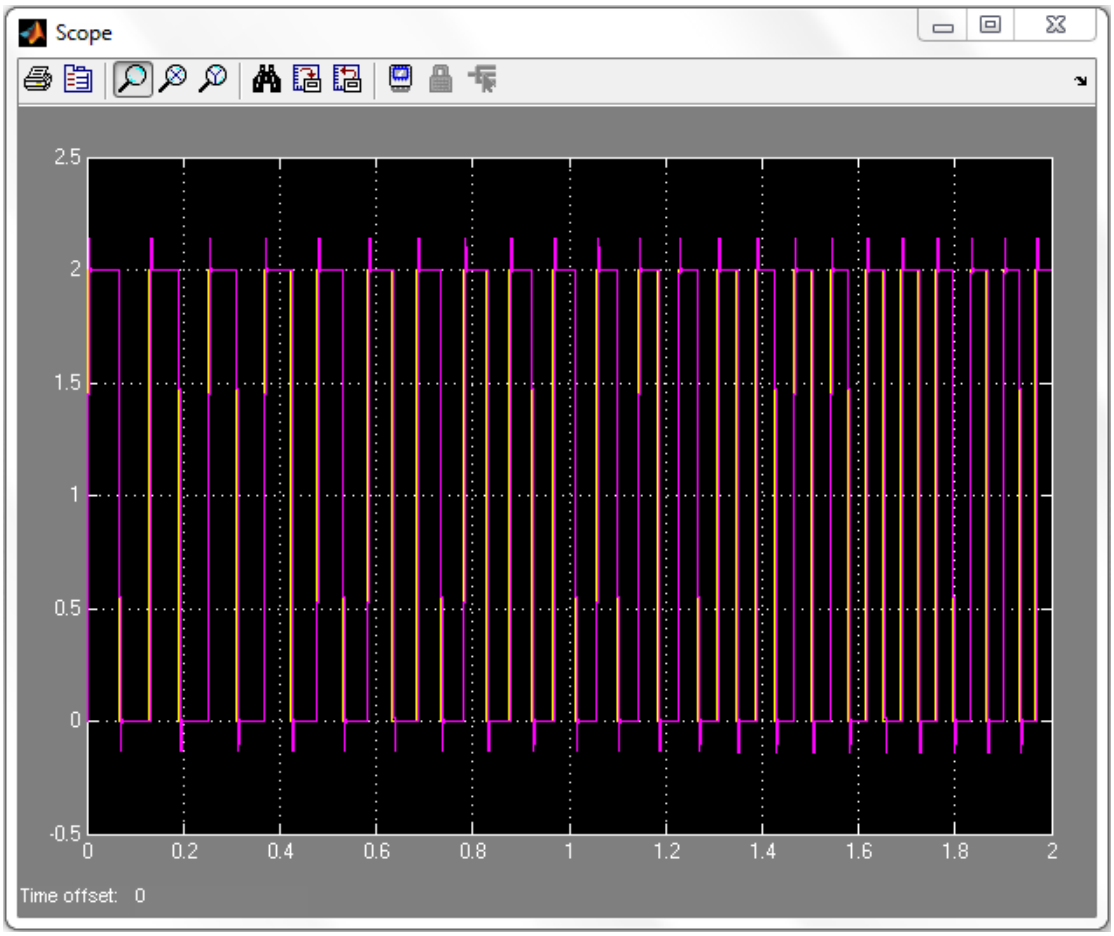

Figure 3.11 System response for varying frequency fixed amplitude input using the discrete PID controller

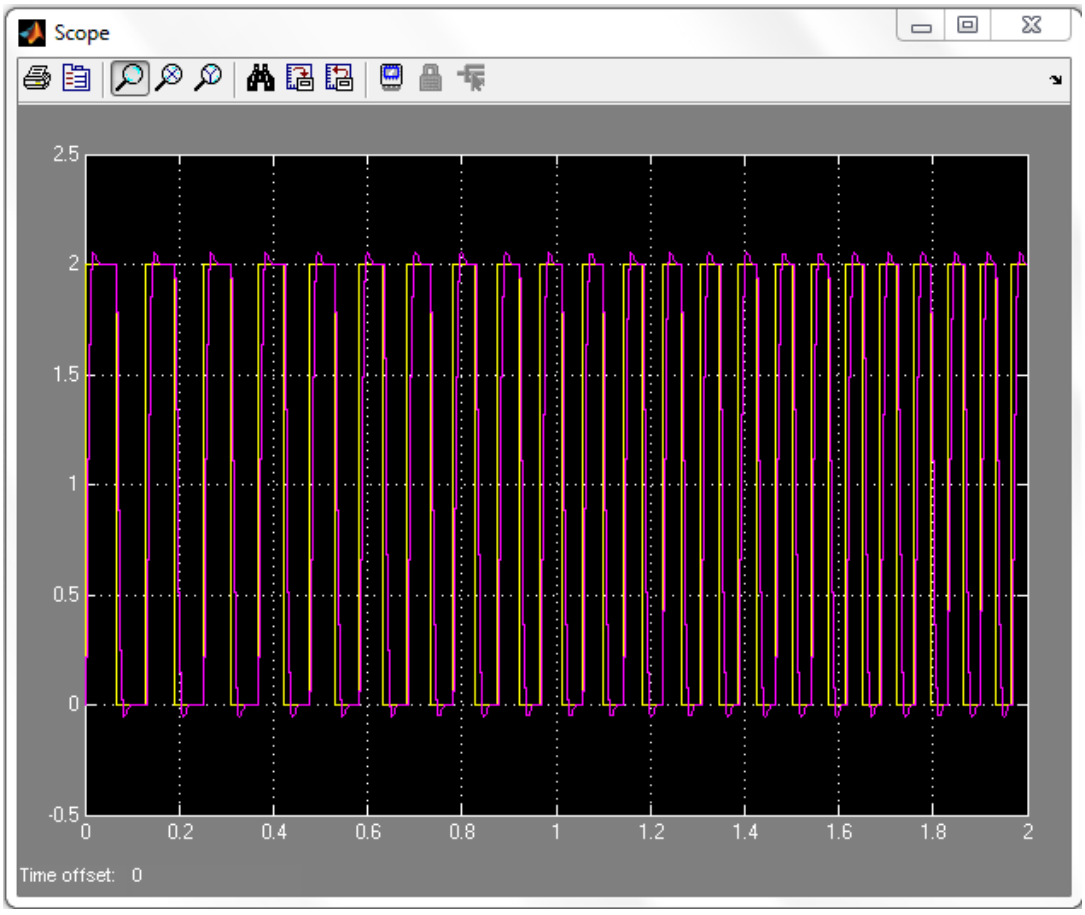

Figure 3.12 System response for varying frequency fixed amplitude input using the inbuilt PID controller block

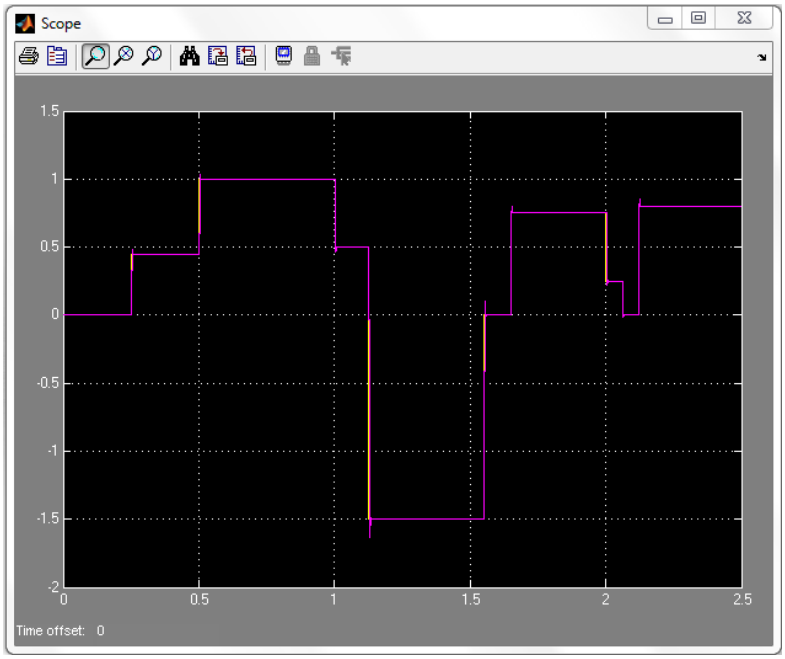

(a)

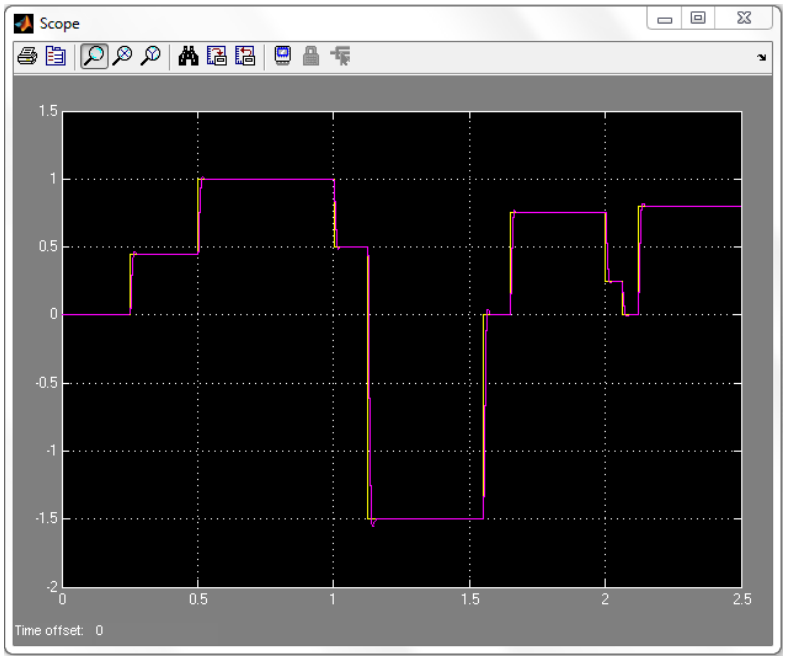

(b)

Figure 3.13 System response for predefined time and amplitude input (a) Output using the discrete PID controller (b) Output using the inbuilt PID controller block

The synchronization of the video frames with the controller output is necessary so that the frames are captured after the output from the controller has settled and the platform is in line with the road surface as well compensation of the car movement.

In all the cases seen above, the requirements for the motor position control in real time are satisfied and hence it can be concluded that this approach for the jitter reduction in video data is valid and can be implemented for the system.

CHAPTER 4

3D RECONSTRUCTION OF ROAD PROFILE

This chapter describes the simulation of a wide line laser, gyroscope and accelerometer for purposes of reconstructing the road profile in 3D. Laser and accelerometer data obtained from profile certification tests carried out at the Texas Transportation Institute (TTI), (Texas A&M) test track was used for certification. Simulated values were used for the gyroscope and other accelerometer sensors since experimental data was not available.

An experiment was done for verifying existence of a linear relationship between two accelerations measured at two ends of a straight line or a rigid body. Description and results of this experiment are also included in this chapter.

4.1 Linear relationship between accelerometers on a straight line

The cost of implementing any project is one of the major factors to take into consideration. Using high tech sensors ensures accurate results but any steps toward cost reduction and making it more cost effective will be advantageous.

There is a linear relationship between two accelerometers on a straight line or a rigid body and only two accelerometers needs to be used for the profile measurement system. An experiment was first carried out to verify this relationship so that prediction of acceleration at any point between two known accelerations can be made.

4.1.1. Accelerometer experiment

The experiment performed to check the linear relationship discussed in the previous section includes the use of three accelerometers, a data acquisition module and a wooden block (used for the rigid body on which the accelerometers are mounted – See Figurer 4.1).

The accelerometers were placed at known positions on the wooden block. The accelerometers needed +15 V and -15 V DC voltages for operation which was provided by a power supply. The accelerometer outputs were attached to the analog inputs on the A/D data acquisition module.

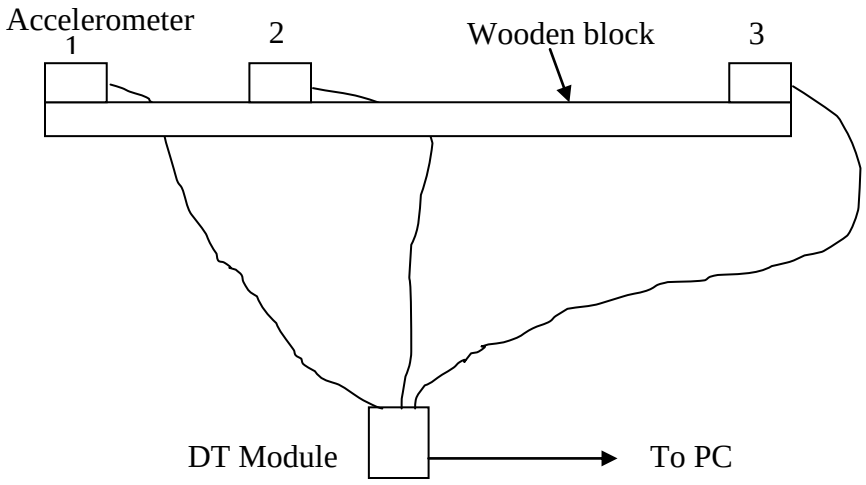

Figure 4.1 Accelerometer experiment setup

Specifications of the apparatus used are given below.

(1) Wooden block -

Dimension 47.5 inches long, 2.5 inches wide and 1.5 inches high

(2) Accelerometers -

Model - Columbia research labs SA-107BHP Single axis linear accelerometer

Operating range - ±15 V

Output voltage range - ±5 V

Range - ±2G, ±4G

(3) Data acquisition module -

Model - Data translation DT9816

Resolution - A/D resolution of 0.30518 mV

Input range - Analog input ranges of ±10V and ±5V

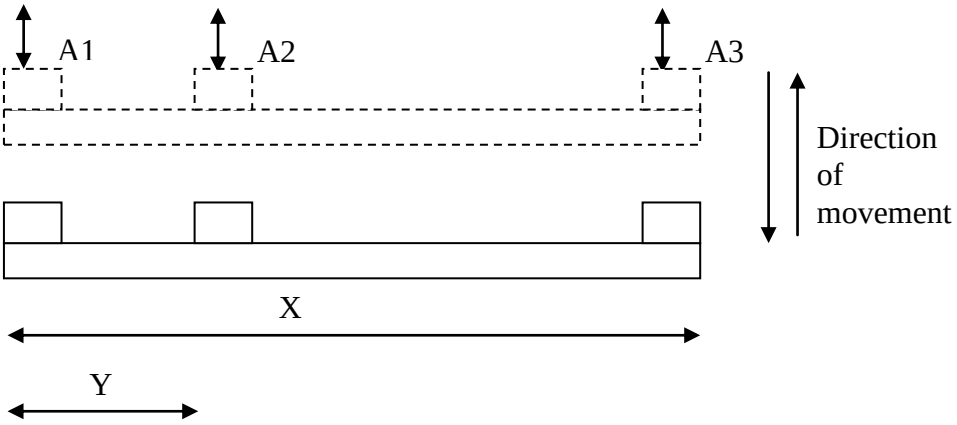

Figure 4.2 Placement of accelerometers and distances between them

As seen from the above figure, A1 is the acceleration measured by the first accelerometer and similarly A2 and A3 are the acceleration measured by the second and third accelerometer respectively. A1 and A3 are separated by the distance X and A2 is at distance Y from A1. The equation $A2 = A1 - \frac{(A1 - A3)Y}{X}$ (4.1) needs to be verified for its validity so that it can be used for predicting accelerations for the lasers not having an associated accelerometer.

The wooden block with the three accelerometers was rotated manually in the direction of the axis measured by the accelerometer. The measured accelerometer readings were recorded using the DT9816 data acquisition module. A Matlab program was written to verify the linear relationship from the recorded data. The error between the actual and predicted readings was computed including the standard deviation and maximum and minimum values of this error. A linear regression was done on the data to get statistical readings to compute the mean and confidence limits of the relationship readings.

The sampling frequency for the data acquisition was set to 300 Hz. The second accelerometer was placed at one fourth distance of the total length from the first accelerometer.

Following are the plots of error in units of the ‘g’ (acceleration due to gravity) readings. The other plots show the movement of all the accelerometers and were obtained by using trapezoidal rule for numerical integration to get the values of the acceleration.

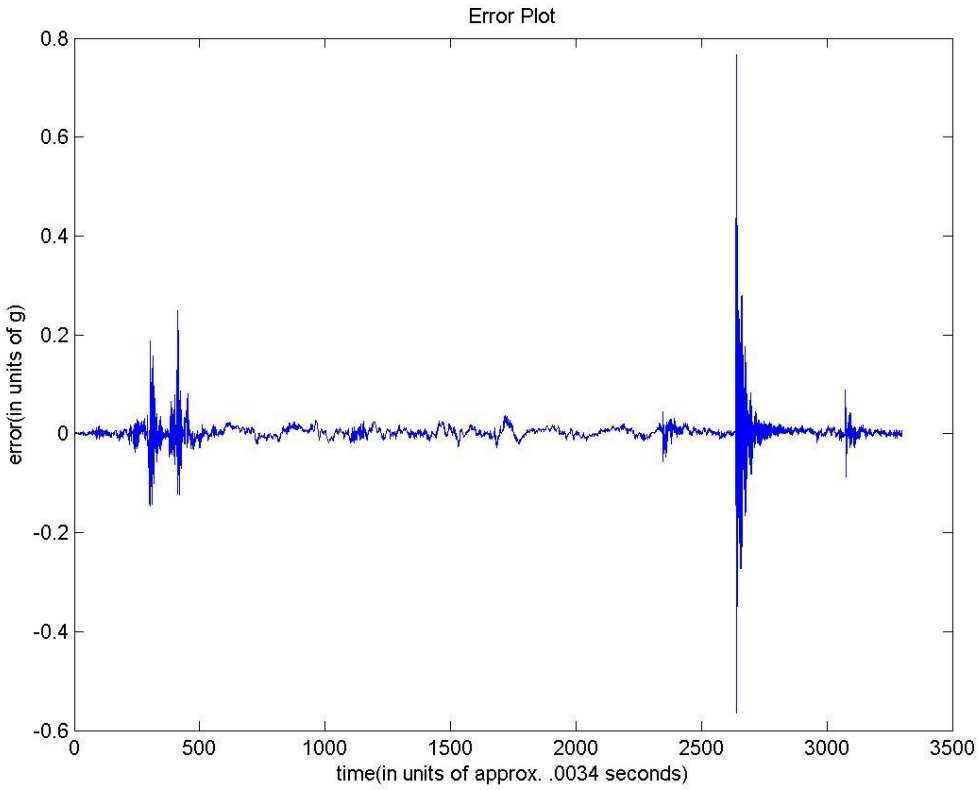

Figure 4.3 Plot for error between practical and theoretical value

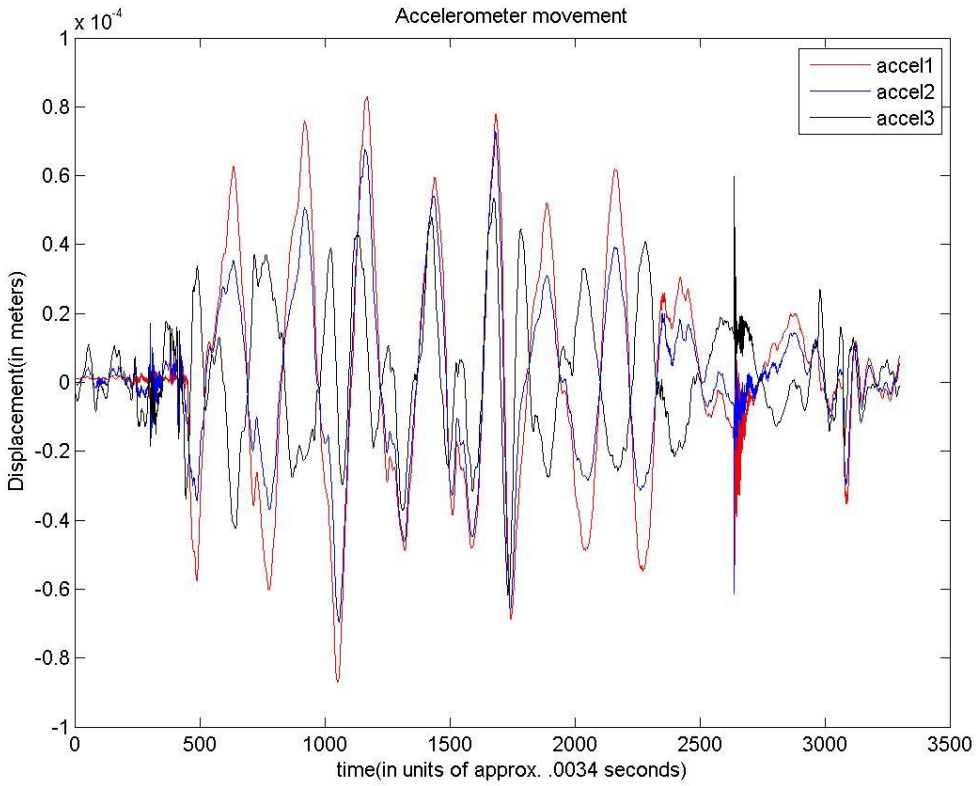

Figure 4.4 Plot showing the movement of the three accelerometers

Average error and standard deviation as calculated with help of matlab are 0.0029g and 0.0315g respectively. Results for regression analysis are shown in the table below.

Table 4.1 Regression statistics

Regression Statistics	
R Square	0.830277203
Standard Error	0.080582317
Observations	4311

R-Squared is a statistical term saying how good one term is at predicting another. The table shows the value of R square to be 0.8302 which states that the two end accelerations are

83.02% reliable for predicting the middle acceleration value. Standard Error between actual and predicted values is 0.08 units and there were total 4311 observations taken in consideration.

From the above results it was verified that the equation 4.1 gives a valid linear relationship. The errors illustrated appeared reasonable for the setup used in the experiment. This relationship can be used to predict acceleration for all the points between the two accelerometers and the requirement for having an accelerometer for each of the lasers is eliminated.

4.2 3D Reconstruction of road profile

As mentioned in earlier chapters the 3D profile will be more advantageous and will give more details about the road than just a normal 2D longitudinal profile. This section provides an explanation of simulation of the wide line lasers and 3D profile development.

3D reconstruction can be successfully carried out by having the data from the wide line laser, gyroscope and the accelerometer. The wide line lasers are not yet available in the marketplace, so simulation of a wide line laser was done with the help of roline laser data taken during test runs carried out by Texas Transportation Institute (TTI) at their test track for the purpose of laser certification.

The roline laser which is a wide line laser having a footprint of about four inches, works in a free mode and a bridge mode. Free mode is where readings for each of the laser points emitted from the roline laser are obtained. The Bridge mode uses an algorithm to compute a representative value of the laser points of a single scan of the roline laser. Free mode data can be made into multiple copies and put together to simulate a wider line laser than the roline laser. The data used for the simulation was a sub-sampled set and consisted of 80 laser points out of the total 196 laser points.

Accelerometer data collected during the same test runs mentioned above was used in the simulation. Simulation of other accelerometers placed at various locations on the bar on which the lasers would be placed can be done using this accelerometer data. Using the linear

relationship between two accelerometers the acceleration at any point between them can be predicted.

The gyroscope data was not available and so the simulation of gyroscope data was required. For the purpose of simulating the gyroscope, an arbitrary value for the cross slope of the road in the transverse direction is taken and applied to the road profile.

A Matlab code was developed to combine all of the data and produce a 3D profile of the road. Profile was calculated according to the profiling algorithm described in the 2nd chapter.

For the simulation procedure 3D profile reconstruction free mode data from the Roline wide line laser was used. Eighty points of a single scan were used. The next step was to obtain the accelerometer data associated with each set of free mode points. The third step is to remove any invalid values in the data, typically at the end points of each data set, and replace the invalid values with neighboring valid data. Predicted accelerometer readings at locations with laser readings without an associated accelerometer are then computed. Next, multiple copies of the laser data are created so it appears like data from a much wider line laser. By using the profiling algorithm on all of the transverse laser points along with the corresponding acceleration provides a 3D profile. The last step is to add the gyroscope data simulation. A constant cross slope is assumed and the 3D profile is tilted at the specified angle.

The simulation was carried out for the data taken at the TTI test track for a 13 meter longitudinal section using a cross slope of 10 degrees. By following the above mentioned procedure the 3D profile was obtained and found to closely match the true profile of the test track.

The results of the simulation are as shown below:

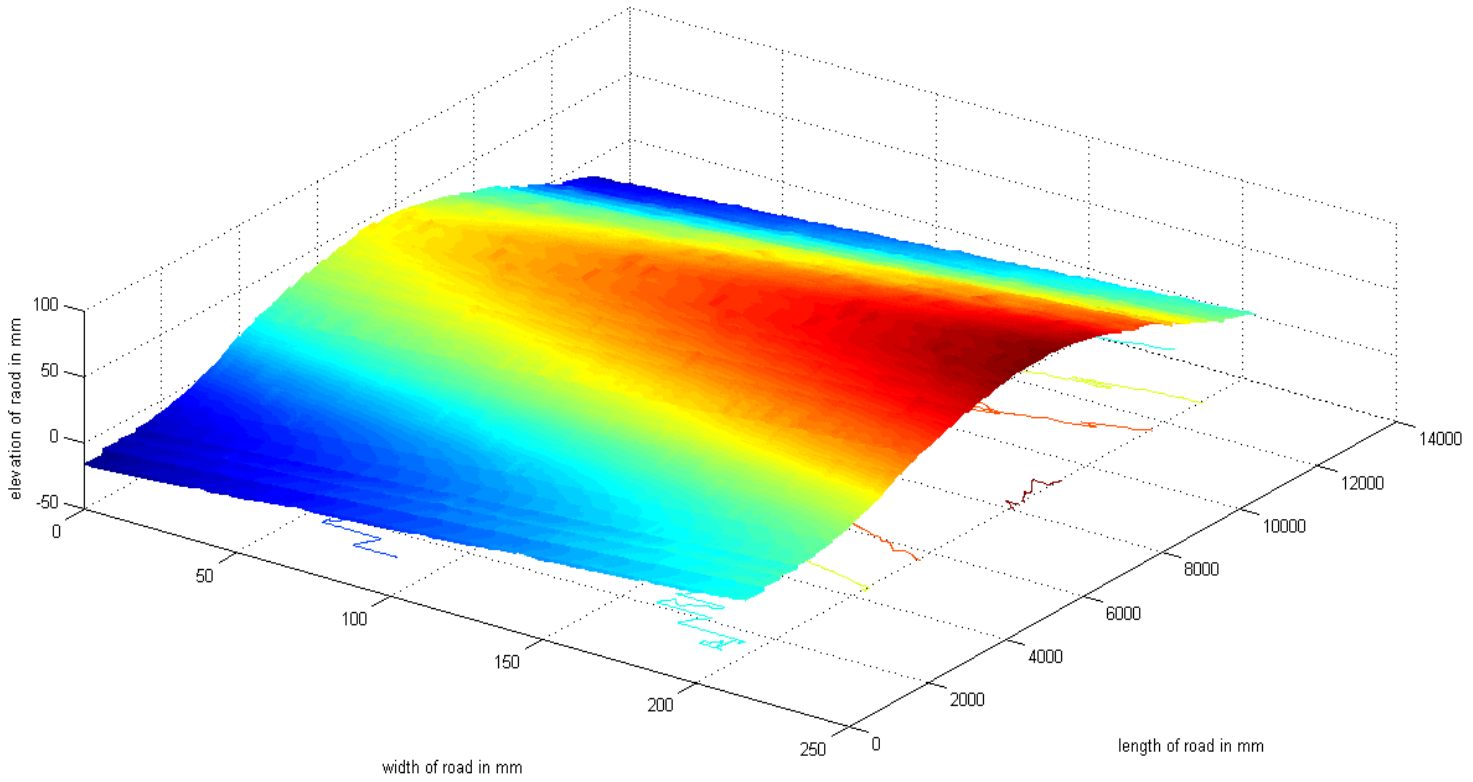

Figure 4.5 Angled view of 3D profile of TTI test track

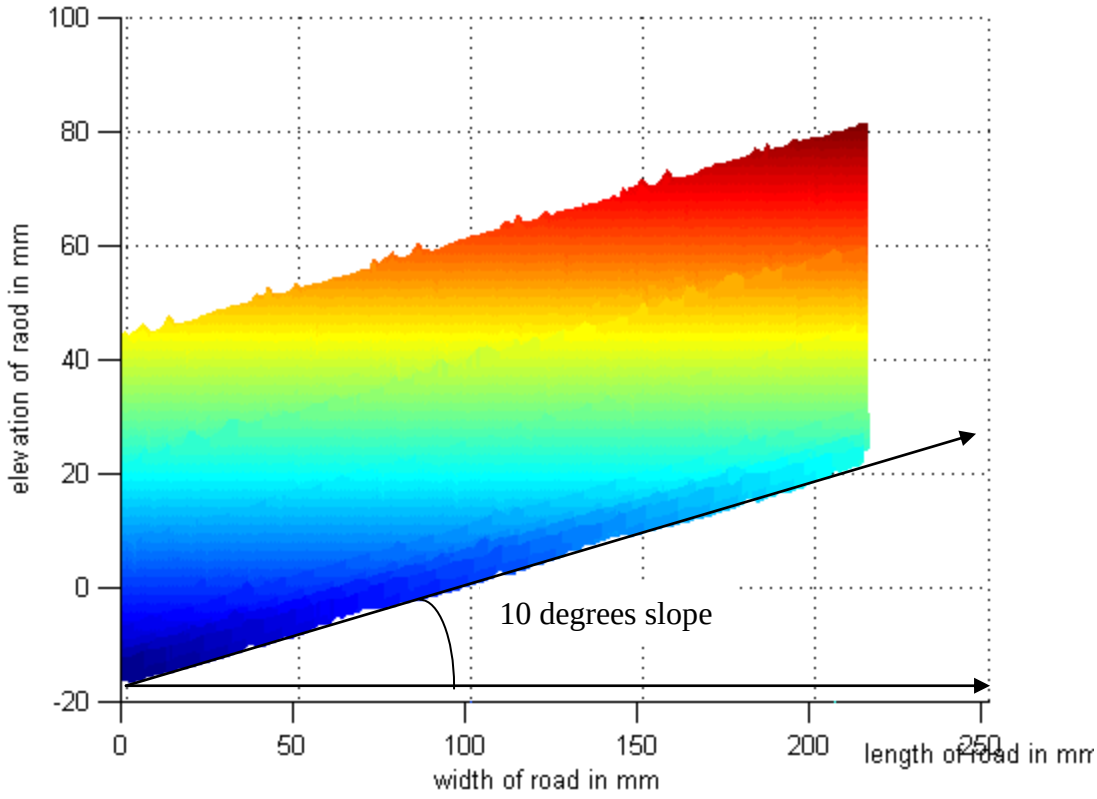

Figure 4.6 Transverse view of 3D profile of TTI test track

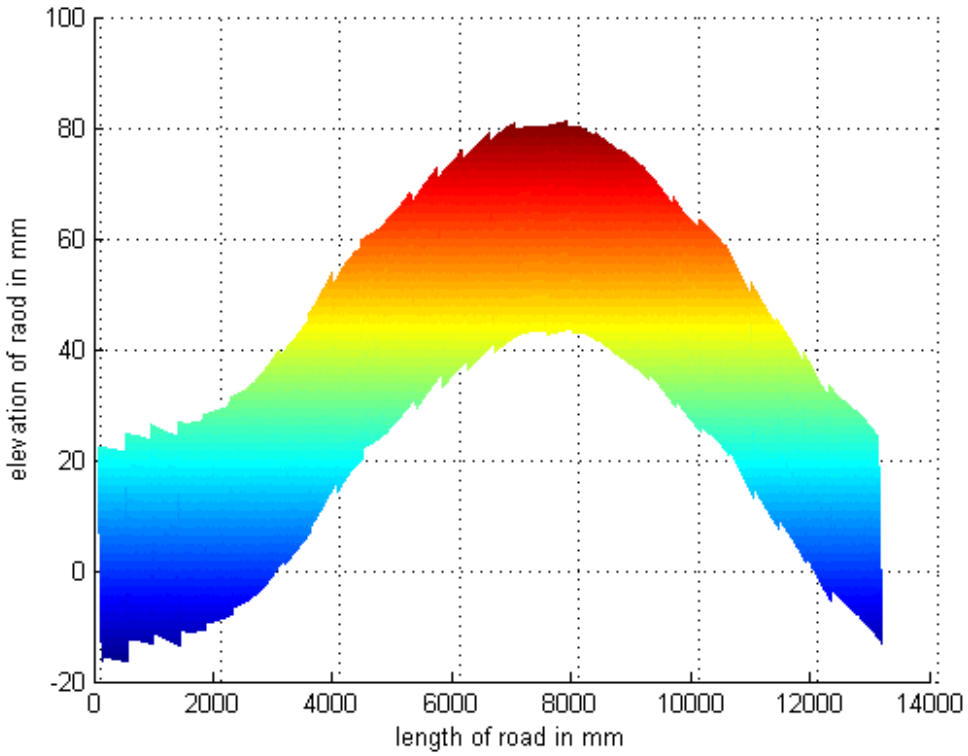

Figure 4.7 Longitudinal view of 3D profile of TTI test track

CHAPTER 5

CONCLUSIONS AND FUTURE WORK

This thesis has presented an investigation of a 3D bridge monitoring system as a novel way for health monitoring of bridges, overpasses and roadways at highway speeds.

The need for getting the video information of the bridge structures with minimum jitter while following the road profile was explained and a control system for real time positioning of a camera platform was introduced. Simulation was performed for checking the feasibility of using PID controllers for the task of platform stabilization. The results of the simulation provided insights into this method and a limited form was implemented.

With the help of an experiment the validity of the relationship between two accelerometers mounted on a rigid body on was verified. This eliminates the need for accelerometers for all lasers.

A successful simulation of wide line lasers using data from the four inch wide line laser was performed, and a 3D profile for a section of TTI test track was developed. Multiple traces from the wide four inch line laser were used to implement a much wider area than the foot print of the roline laser providing 3D transverse and longitudinal profile. An implementation of these lasers helps improve the analysis of the road surface and condition.

Research has been done for image processing techniques and algorithms that can be used for finding changes in the bridge structures. The research included development of a framework that could be used for data collection for 3D profiling.

The 3D bridge monitoring system has not been fully evaluated and so work is needed for implementation and wide scale usage. Additional research is needed for the evaluation of

computer vision techniques for comparison of the video data, designing a platform having capabilities of pitch and yaw rotation for mounting the camera, development of a program for real time 3D profile measurement and evaluation of different real time operating systems suitable for this application.

REFERENCES

[1] R. Huang, I. Mao and H. Lee, "'Exploring the Deterioration Factors of RC Bridge Decks: A Rough Set Approach," *Computer-Aided Civil and Infrastructure Engineering*, vol. 25, no. 7, pp. 517-529.

[2] K. Wardhana and F.C. Hadipriono, "'Analysis of Recent Bridge Failures in the United States," *J.Perform.Constr.Facil.*, vol. 17, no. 3, 08/00, pp. 144-150.

[3] *Insight: non-destructive testing and condition monitoring*, British Institute of Non-destructive Testing, Northampton, England, 1997.

[4] M.W. Sayers, S.M. Karamihas and University of Michigan, *The little book of profiling: basic information about measuring and interpreting road profiles,* Transportation Research Institute, 1998.

[5] *Annual book of A.S.T.M. standards*, American Society for Testing and Materials, 2007.

[6] R.S. Walker, E. Fernando, E. Becker, J.A. Qader and G. Harrison, "'USING PROFILE MEASUREMENTS TO LOCATE AND MEASURE GRIND AND FILL AREAS TO IMPROVE PAVEMENT RIDE,", vol. FHWA/TX-08/0-4463-1 Report 0-4463-1, 2008.

[7] K. Lopez, *Control Systems- Digital Systems*, Netlibrary Inc, 2008.

[8] A. Visioli, *Practical PID control*, Springer, New York, NY, 2006.

[9] H. Ozbay, *Introduction to feedback control theory*, CRC press, Palm Beach County, Florida, 1999.

[10] *InTech,* Instrument Society of America, Durham, NC, 1996.

[11] T. Wescott, *PID without a PhD*, http://www.embedded.com.

[12] J.N. Chiasson, *Modeling and high performance control of electric machines*, John Wiley, Hoboken, NJ, 2008.

BIOGRAPHICAL INFORMATION

Digant Shah was born in Gujarat, India in 1987. He received the Bachelor of Engineering in Electronics and Communication Engineering from Gujarat University in 2009. He enrolled in the Master of Science in Electrical Engineering program at The University of Texas at Arlington (UTA) in 2009. While studying at UTA, he did various projects in the field of microprocessor systems and embedded systems. He started his research at the Transportation and Instrumentation Laboratory in the CSE department of UTA. His research interests include embedded microcontroller systems, FPGA and 3D road profiling.